Chang *et al. Energy Mater* 2024;4:400052
DOI: 10.20517/energymater.2023.143

Energy Materials

Article

Open Access

Check for updates

Evaluation of asymmetric poly(vinylidene fluoride)-coated polyimide separator with three-dimensionally homogeneous microporous structure for high-safety lithium-ion battery

Hui Chang[1,#], Guohong Kang[1,#], Zengqi Zhang[2,*], Wei Liu[1,*], Yongcheng Jin[1,*]

[1]School of Materials Science and Engineering, Ocean University of China, Qingdao 266100, Shandong, China.
[2]Qingdao Institute of Bioenergy and Bioprocess Technology, Chinese Academy of Sciences, Qingdao 266101, Shandong, China.
[#]Authors contributed equally.

***Correspondence to:** Prof. Yongcheng Jin, School of Materials Science and Engineering, Ocean University of China, No. 1299 Sansha Road, New Xihaian District, Qingdao 266100, Shandong, China. E-mail: jinyongcheng@ouc.edu.cn; Prof. Wei Liu, School of Materials Science and Engineering, Ocean University of China, No. 1299 Sansha Road, New Xihaian District, Qingdao 266100, Shandong, China. E-mail: weiliu@ouc.edu.cn; Prof. Zengqi Zhang, Qingdao Institute of Bioenergy and Bioprocess Technology, Chinese Academy of Sciences, No. 189 Songling Road, Laoshan District, Qingdao 266101, Shandong, China. E-mail: zhangzq@qibebt.ac.cn

How to cite this article: Chang H, Kang G, Zhang Z, Liu W, Jin Y. Evaluation of asymmetric poly(vinylidene fluoride)-coated polyimide separator with three-dimensionally homogeneous microporous structure for high-safety lithium-ion battery. *Energy Mater* 2024;4:400052. https://dx.doi.org/10.20517/energymater.2023.143

Received: 30 Dec 2023 **First Decision:** 3 Apr 2024 **Revised:** 17 Apr 2024 **Accepted:** 26 Apr 2024 **Published:** 24 May 2024

Academic Editor: Jinqiang Zhang **Copy Editor:** Fangling Lan **Production Editor:** Fangling Lan

Abstract

Safety hazards associated with separators in lithium-ion batteries are more pronounced in light of the significant improvement of energy density of batteries, hindering their wide application. In this research, asymmetric poly (vinylidene fluoride) (PVDF)-coated polyimide separators with three-dimensionally homogeneous microporous (3DHM API/PVDF) structure are prepared, in which a PVDF layer with a thickness of 6 μm on one side of polyimide. Polyimide, as the base film, has a high heat-resistant temperature which ensures that as-prepared separators will not be shrunk and burned. The coated PVDF layer imparts 3DHM API/PVDF with thermal shutdown function at 175 °C due to the melting of PVDF. The temperature difference between the shutdown and meltdown temperature is over 100 °C, ensuring that the LIB assembled with 3DHM API/PVDF is safe for use. Moreover, the interconnected microporous structure of the separator facilitates the formation of 3D Li^+ transport pathways and uniformity of lithium deposition, suppressing lithium dendrite growth. The coin cells assembled by 3DHM API/PVDF exhibit similar electrochemical performance to that of a commercial polypropylene separator at

room temperature. Therefore, the novel 3DHM API/PVDF separator may be a promising candidate for a significantly safer LIB.

Keywords: Composite separator, flame resistance, shutdown function, functional polymeric coating, three-dimensionally homogeneous microporous structure, lithium-ion battery

INTRODUCTION

Recently, lithium-ion batteries (LIBs) have become indispensable power sources for portable electronics and electric vehicles owing to their high energy density, extended service life, and minimal self-discharge[1]. However, their safety concerns have been the primary hindrances impeding their widespread applications. To address the above issues, numerous strategies have been implemented, including using flame retardant additives[2], advancing separator designs[3,4], enhancing electrode protection[5,6], and developing all-solid-state electrolyte membranes[7]. The separator employed in LIBs, serving as an ionic conductor while functioning as an electronic insulator, exerts a notable influence on their performances, particularly with regard to safety and power density[3,8]. A suitable separator for large-scale LIBs with high safety standards should possess optimal porosity and outstanding wetting performance to facilitate enhanced ion transport and reduced cell impedance. Furthermore, it should exhibit excellent thermal endurance, preventing shrinkage or melting[9,10]. When the LIBs are operated at elevated temperatures, several exothermic reactions are easily induced, including decomposition of the solid-electrolyte interface (SEI), parasitic reactions of the electrolyte, and internal short circuits. Although the decomposition of SEI and electrolyte leads to heat accumulation in LIBs, the rate of temperature increase in the cells is acceptable. However, the internal short circuit triggered by separator shrinkage generates a large short-circuit current, resulting in catastrophic heat accumulation and temperature increase of LIBs. Separators are the main components of cells that physically separate electrodes and prevent internal short circuits, but their shrinkage or complete collapse inevitably occurs owing to inferior thermal stability. Consequently, it is of paramount importance to optimize the stability of the separator under elevated temperatures to enhance the safety performance of LIBs.

Porous polyolefin separators, composed of polyethylene (PE), polypropylene (PP), and their composites such as triple PP/PE/PP separators and PP/PE, are currently the most prevalent in the field of LIBs. These microporous membranes exhibit attractive qualities, such as superior chemical properties, outstanding mechanical strength, and low cost. However, their poor thermal stability is one of the most significant factors that result in safety hazards of batteries. Specifically, PE and PP separators exhibit melting points of 140 and 165 °C, respectively[11], and partly shrink or completely collapse at elevated temperatures, leading to high short-circuit current and catastrophic thermal runaway. During the past decades, considerable research has been devoted to improving thermal stability of separators, such as developing those with novel materials and modifying them with high melting-point polymers[12-15]. Mitsubishi Paper Japan developed non-woven fabric separators with high dimensional stability at 180 °C[16]. The coin cell of $LiMn_2O_4$/Graphite using as-prepared separators showed superior rate and cycle performance than a cell with PP separators, resulting in a discharge capacity of 16 mAh for non-woven fabric separators, significantly surpassing the 6.5 mAh capacity achieved with PP separators. Teijin Limited Japan reported the development of aramid-coated fine porous PE separators, which exhibit significantly enhanced heat shrinkage tolerance over 250 °C. Moreover, these separators possess the same shutdown function as PE fine porous separators and do not experience meltdown at temperatures below 200 °C[17]. The atomic layer deposition technique is used to modify the surface of polyolefin-based separators, and it is found that after depositing 100 layers, the thermal shrinkage of as-prepared separators at 180 °C was less than 1%. Furthermore, the cells with as-prepared separators demonstrate a superior rate performance and improved capacity retention over 100 cycles compared to bare membranes[18].

Due to its high thermal stability, polyimide (PI) has been increasingly used as a single polymer membrane[11,19-24] to improve thermal stability of batteries. Although PI separators increase safety performances at thermal abuse conditions, they show a negligible effect on relieving heat release under electrochemical abuse, such as serious overcharge. Thermal shutdown separators automatically cut off transport paths of Li^+ at elevated temperatures, inhibiting rapid heat accumulation in batteries[25]. Sun *et al.* prepared a novel three-layer separator[20]. Polybenzimidazole-sheath@polyimide-core nanofibers (PBI@PI) with high strength provide structural support and keep dimensional stability at elevated temperatures. While PBI nanofibers melt at high temperatures, they act as a barrier to the transport of Li^+, thereby providing a shutdown function for the separator. Wu *et al.* reported on sandwich-type PI/Poly (vinylidene fluoride) (PVDF)/PI separators prepared by electrospinning, which combines the advantages of PI and PVDF[22]. The PI outer layers demonstrate excellent thermal stability, while the interlayer of PVDF can melt and form a non-porous film that effectively shuts down the battery. However, compared with interconnected macroporous nanofiber structure, three-dimensionally homogeneous microporous (3DHM) materials have interconnected microporous structure, facilitating formation of 3D Li^+ transport paths and uniformity of lithium deposition[26,27]. Moreover, ultrathin pore walls ensure the entire surface is modified uniformly[28-30].

We wonder whether there is a strategy that combines 3DHM structure, functional polymeric coating and thermally stable membrane that can be employed to prepare a separator suitable with thermal shutdown function for high-safety LIBs. Based on the design mentioned above, SiO_2 nanoparticles (300 nm) were introduced and then etched by hydrofluoric acid (HF) to form 3DHM structure. Functional PVDF coating with a thickness of 6 μm can melt and form an insulating film to close pores and block ion transfer at high temperatures, terminating the electrochemical process under abuse conditions. A single polymer membrane comprising PI with a thickness of 17 μm and a highly porous structure was utilized. The membrane exhibited high thermal stability. As a result, the asymmetric 3DHM cross-linked PVDF-coated polyimide (3DHM API/PVDF) separator exhibits good thermal stability and shutdown functions. The interconnected microporous structure of the separator facilitates formation of 3D Li^+ transport paths and uniformity of lithium deposition, suppressing lithium dendrite growth.

EXPERIMENTAL

Materials: PVDF, Methyl-2-pyrrolidone (NMP), and Poly(vinylidenefluoride-hexafluoropropylene) (PVDF-HFP) were purchased from Aladdin Industrial Co, China. Sulfolane was purchased from Meryer (Shanghai) Biochemical Technology Co., Ltd. HF (48.0%-55.0% w/w in water) was obtained from Energy Chemical. Spherical silica particles (300 nm) were obtained from KE-S30, Nippon Shokubai. $LiNi_{0.8}Co_{0.15}Al_{0.05}O_2$ (NCA) was purchased from Guangdong Canrd New Energy Technology Co., Ltd. The supplier of lithium foil was China Energy Lithium Co., Ltd. The electrolyte of LB-158 (1 M $LiPF_6$ in Ethylene carbonate: Dimethyl carbonate = 3:7 Vol% with 2% Vinylene carbonate) was obtained from DoDo Chem. The porous PI film with 50%-70% porosity was purchased from Jiangxi Advanced Nanofiber S&T Co., Ltd. The above-mentioned raw materials were not subjected to any further treatment after purchase. PP (Celgard 2500) and PP/PE/PP (Celgard 2325) were supplied by Suzhou Sinero Technology Co., Ltd.

Preparation of 3DHM API/PVDF separators: The 3DHM API/PVDF separator was fabricated by etching a silica-based sacrificial template. PVDF and silica particles were placed in an oven at 60 °C for an hour before use. Additionally, 0.5 g PVDF was dissolved in 2 g NMP to obtain a clear solution. Then, 0.5 g silica particles were added to the solution, and the mixture was stirred to obtain a homogeneous slurry. The final slurry was cast onto porous polyimide film with a coating thickness of 5-10 μm and subjected to a vacuum oven drying process at 60 °C for 12 h to obtain an asymmetric composite membrane consisting of porous

PI, SiO_2 and PVDF, denoted as API/PVDF-SiO_2. The template SiO_2 was removed by HF, and the obtained asymmetric membrane with 3DHM structure was washed thoroughly with deionized water, marked as 3DHM API/PVDF. The resulting membrane was then placed in a vacuum oven at 60 °C for 12 h to ensure evaporation of the water. The fabricated separator was cut into circles with diameters of 16 mm and stored in a glove box for further characterization.

Characterizations: The surface and cross-section morphologies of all these asymmetric separators and lithium metal were observed by a scanning electron microscope (SEM, Zeiss Gemini300). The thermogravimetric analysis (TGA) was conducted using a PerkinElmer simultaneous thermal analyzer (STA 6000). The heating rate was 10 °C min^{-1} in a nitrogen atmosphere. The thermal shrinkage of the separator was determined from the dimensional changes after thermal treatments for 30 min from 50 to 275 °C. The degree of thermal shrinkage was calculated by: Shrinkage = $(A_0 - A_1)/A_0 \times 100\%$, where A_0 and A_1 are the areas of the separator before and after thermal treatment. The tensile strength of the separators (with a size of 10 mm × 100 mm) was measured using an electronic universal testing machine (MTS E43.104) with a tensile speed of 1 mm S^{-1}. The porosity and pore-size distributions of the separators were analyzed using a mercury porosimeter (Conta PoreMaster 33). The contact angle of the membrane was measured on CSCDIC-200S (Sindin, Dongguan). PP and 3DHM API/PVDF separators were immersed in liquid electrolyte for three min to measure liquid electrolyte uptake. The separators were then quickly weighed after removing any excess solution using filter paper. The experiment utilized circular samples with a 16.5 mm diameter. Electrolyte uptake was calculated by: Electrolyte uptake = $(W_1 - W_0)/W_0 \times 100\%$, where W_1 represents the weight of the electrolyte-soaked separator and W_0 represents the weight of the unsoaked separator. The ionic conductivity of the membranes was tested by sandwiching them between two stainless steel electrodes and calculating it using: $\sigma = L/RS$. Here, σ is the ionic conductivity, L represents the separator thickness, R is the bulk resistance, and S is measured membrane area. The electrochemical impedance spectroscopy (EIS) method using SP-300/240 (Bio-Logic SAS) was used to determine R. EIS was recorded using an alternating current with an amplitude of 5 mV from 7 MHz to 0.1 Hz. The measurements were taken at different temperatures after being stored in a pre-set hot-air oven for 30 min. LB-158 and 0.5 mol L^{-1} LiTFSI in sulfolane were used as the electrolyte for 25 °C and high temperature ionic conductivity tests, respectively. The NCA cathode slurry was prepared by blending NCA powder with PVDF and Super-P in an 8:1:1 weight ratio in NMP. The resulting mixture was coated onto an aluminum foil current collector and dried in an oven at 120 °C for 12 h to produce the NCA cathode plate. The cathode plate of NCA was cut into round segments with a diameter of 12 mm. Approximately 1 mg cm^{-2} of cathode active materials is loaded. To investigate the electrochemical properties of the battery, a 2032-type coin cell has been assembled using commercial PP (Celgard 2500) or 3DHM API/PVDF separators between the lithium anode and the NCA cathode. The assembly of the battery begins with the placement of the lithium foil within the negative shell. This is followed by adding about 30 μL of liquid electrolyte and separator. Subsequently, 20 μL of liquid electrolyte is added to the separator, after which the NCA cathode, stainless steel gasket, and shim are placed within the negative shell in that order. Finally, the positive shell is covered, and the battery is sealed using a sealing machine. The procedure for assembling Li/separator/Li cells was identical to that previously described, with the exception of the substitution of NCA with lithium foil. A dry argon glove box (O_2 < 0.1 ppm, H_2O < 0.1 ppm) assembled the cells. The charging and discharging data were measured using the LAND battery system.

RESULTS AND DISCUSSION

The manufacturing process of the 3DHM API/PVDF separator is shown schematically in Figure 1. The slurry composed of PVDF/SiO_2 nanoparticles was cast on the porous PI film, and the resulting film was denoted as API/PVDF-SiO_2. After the etching of silica by HF, the 3DHM API/PVDF separator formed. The

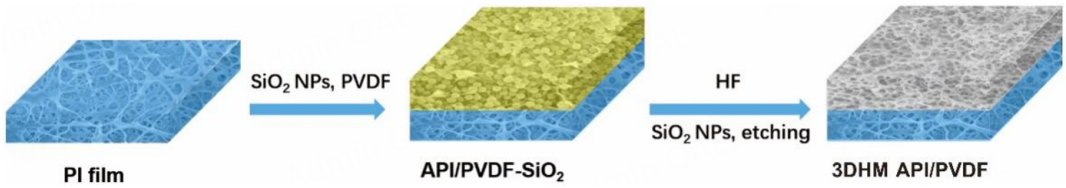

Figure 1. Schematic of the preparation of 3DHM API/PVDF separator.

separator structures and properties are of paramount importance in the battery performance[31]. The pristine PI film consists of interlinked branches with a pore size of 0.5-2 μm [Figure 2A]. Figure 2B-F illustrates the superficial and cross-section SEM images of both sides of API/PVDF-SiO_2. The unmodified side of the API/PVDF-SiO_2 [Figure 2B] remained the structure of the pristine PI film, and the modified side was fully covered with SiO_2 nanoparticles [Figure 2C], clearly distinguishing it from the pristine PI film. From the cross-sectional images [Figure 2D-F], the unmodified and modified layers exhibit loose and dense characteristics, respectively.

In the further steps, API/PVDF-SiO_2 was etched in HF to remove the template of SiO_2, generating porous structure. As displayed in Figure 3A, the surface of the unmodified side preserves the porous structure of the PI membrane. The layer that has been modified exhibits a uniform porous structure with a pore size of approximately 300 nm [Figure 3B and C]. These pores are arranged orderly on a large scale, and the 3DHM API/PVDF with a smooth surface retains the integrity of API/PVDF-SiO_2 [Figure 3D-F], indicating that the etching process does not destroy the original structure. The thickness of the PVDF coating is about 6 μm. The smooth surface and uniform thickness of the PVDF coating layer contribute to a superior interface with electrodes and ensure an adequate flow of electrolyte which are essential elements for the practical applications of lithium batteries. Moreover, 3DHM in the membrane can form lots of uniform paths for Li^+ transports, and facilitate homogeneous Li dispersion at anodes, suppressing lithium dendrite growth and enhancing cycling stability.

Thermal stability is a crucial factor in the safe operation of LIBs. TGA-differential scanning calorimetry (DSC) analysis of 3DHM API/PVDF separators indicates a heat flow change at about 172 °C [Figure 4], corresponding to a melting process of the PVDF layer in 3DHM API/PVDF. A single endothermic peak is observed in the DSC profiles of PP at 165 °C. This is ascribed to melting of PP materials. Similarly, PP/PE/PP displays two distinct heat absorption peaks at 137 and 161 °C, corresponding to the melting of PE and PP, respectively. The DSC results prove that the high thermo-stability of 3DHM API/PVDF is attributed to the PVDF coating and PI film.

The primary function of separators is to prevent the cathode and anode from coming into contact, which can cause electrical short circuits. Additionally, the separators should remain stable within the battery, even in battery-related accidents. Therefore, any thermal shrinkage of the separator can significantly affect the thermal stability of the battery. To evaluate the thermal shrinkage of as-prepared separators, a series of thermal treatments ranging from 50 to 275 °C were carried out for half an hour and the results are shown in Figure 5. PP and PP/PE/PP remained intact below 50 °C, exhibiting no deformation [Figure 5A1 and A2, B1 and B2]. Both PP and PP/PE/PP exhibited varying degrees of heat shrinkage as temperature increased above 100 °C. Specifically, PP exhibited a shrinkage of 2% at 100 °C, which increased to 14.3% at 120 °C, 34.7% at 140 °C, and 42.8% at 160 °C [Figure 5C1-F1]. The shrinkage of PP/PE/PP is comparable to that of PP [Figure 5C2-F2]. At a temperature of 180 °C, the heat shrinking of PP and PP/PE/PP reaches 100%. This is due to the complete melting of PP and PE [Figure 5G1 and G2]. In contrast, the

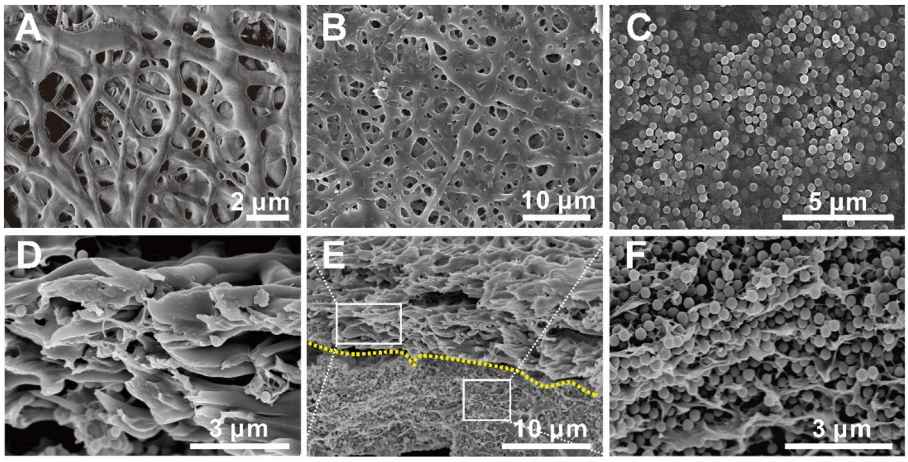

Figure 2. SEM images of (A) the pristine PI film and (B-F) the surface and cross-sectional SEM images of API/PVDF-SiO_2, (B) the unmodified side, (C) the modified side, (D) the upper section, (E) the overall cross-section and (F) the lower section.

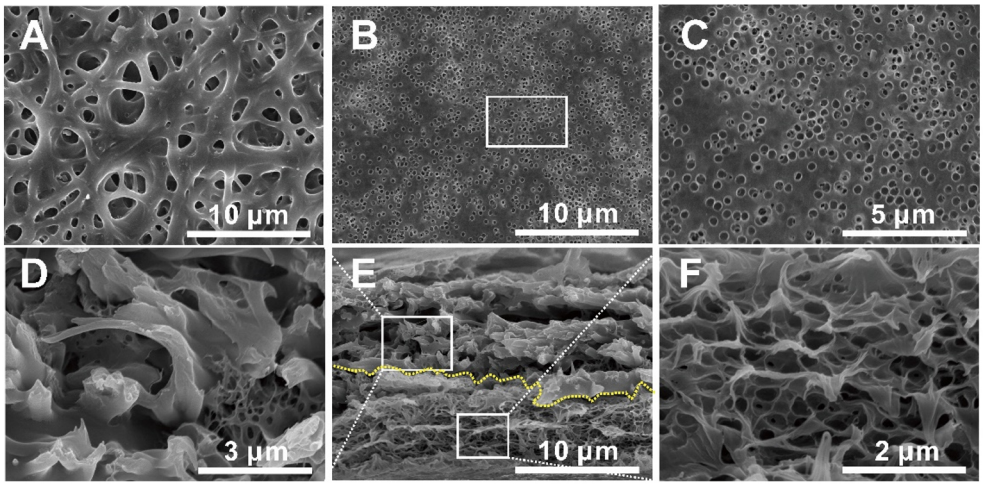

Figure 3. Surface and cross-sectional SEM images of 3DHM API/PVDF separator (A) the unmodified side, (B and C) the modified side, (D) the upper section, (E) the overall cross-section and (F) the lower section.

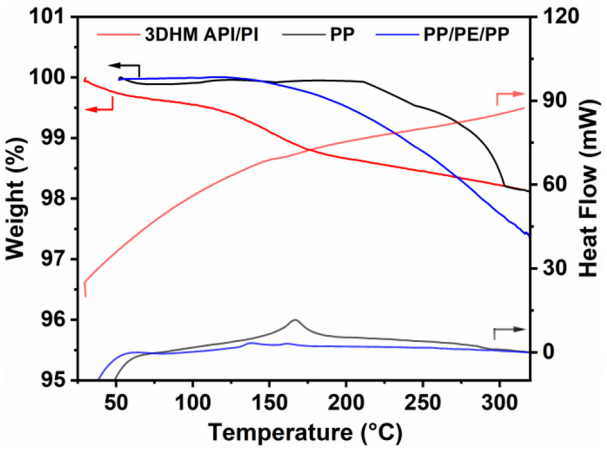

Figure 4. TGA-DSC of PP, PP/PE/PP and 3DHM API/PVDF.

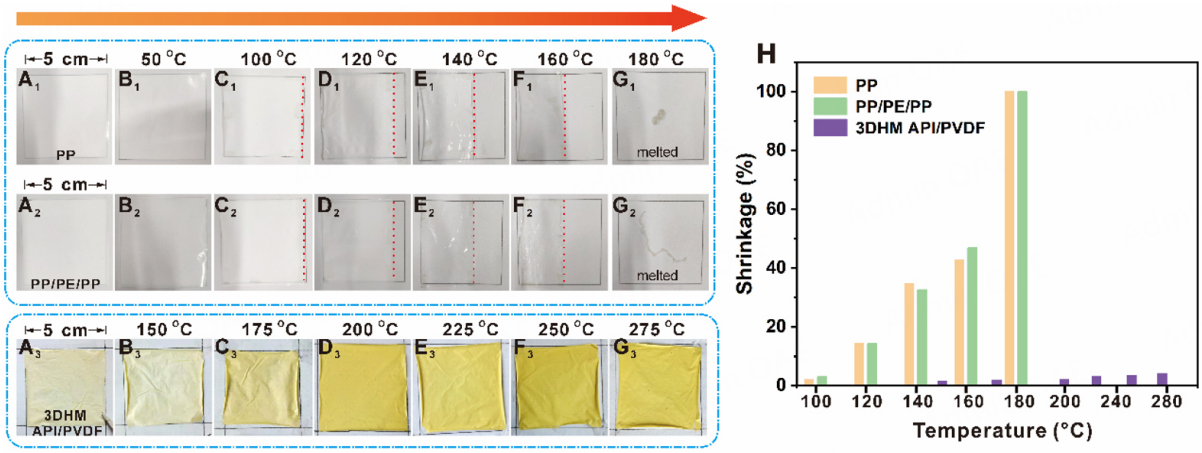

Figure 5. Optical photos and shrinkage of PP, PP/PE/PP and modified layers of 3DHM API/PVDF separators before and after the thermal treatments for 30 min at different temperatures. (A_1-A_3) before the thermal treatment, (B_1 and B_2) 50 °C; (B_3) 150 °C; (C_1 and C_2) 100 °C; (C_3) 175 °C; (D_1 and D_2) 120 °C; (D_3) 200 °C; (E_1 and E_2) 140 °C; (E_3) 225 °C; (F_1 and F_2) 160 °C; (F_3) 250 °C; (G_1 and G_2) 180 °C; (G_3) 275 °C. (H) Shrinkage of PP, PP/PE/PP and 3DHM API/PVDF separators after thermal treatment at different temperatures.

3DHM API/PVDF demonstrated excellent thermal stability. The 3DHM API/PVDF separator presents thermal shrinkage of less than 4% over a wide temperature range of 150 to 275 °C. This is attributed to the application of the high-heat-resistance PVDF coating and PI film. Moreover, the white color of PVDF coating allows for visualization of its melting during the heat treatment process. As illustrated in Figure 5A3, 3DHM API/PVDF separators exhibit a white surface at 25 °C, which aligns with the color of the PVDF. No significant color change was observed following treatment at 150 °C [Figure 5B3]. Upon reaching a temperature of 175 °C, the color of the separator transforms, becoming light yellow due to the partial melting of PVDF [Figure 5C3]. After thermal treatments at 200 °C or higher, the color turns bright yellow [Figure 5D3-G3] because of the complete melting of PVDF. Figure 5H presents the shrinkage of PP, PP/PE/PP, and 3DHM API/PVDF after thermal treatment at different temperatures. Figure 6 illustrates the flame-retardance of separators. The Celgard PP does not exhibit flame-retardance as it burns away immediately upon ignition. In contrast, 3DHM API/PVDF demonstrates self-extinguishing behavior, indicating excellent flame-retardant properties. The 3DHM API/PVDF membrane exhibits excellent dimensional thermo-stability and flame resistance, making it a safer option than PP film for LIB separator applications.

In LIBs, the "shutdown" feature of separators is useful to prevent thermal runaway reactions, limiting further lithium-ion transport through the separator and temperature rise in short-circuited cells[32,33]. The shutdown temperature should be lower than the melting point of the separators, and the difference should be wide enough to prevent internal short circuits[15]. To visualize the shutdown process of 3DHM API/PVDF, the morphologies of the modified layer and unmodified side were imaged by SEM after heat treatment. As shown in Figure 7A1, the modified side of 3DHM API/PVDF exhibits homogeneous pores, and after heat treatment at 150 °C for 0.5 h, the morphology did not change [Figure 7B1]. With increasing heat treatment temperature from 150 to 175 °C, the PVDF partially melted and the pores in the modified side became smaller [Figure 7C1]. When the heat treatment increased to 200 °C or above, the pores disappeared and were blocked by the melted PVDF [Figure 7D1, Supplementary Figure 1]. However, the pores structure of the unmodified side remained unaltered prior to and following the heat treatment [Figure 7A2-D2]. The self-thermal shutdown function of 3DHM API/PVDF blocks ion transport near the thermal runaway temperature, preventing short circuits and thermal runaway of the battery. Moreover, the

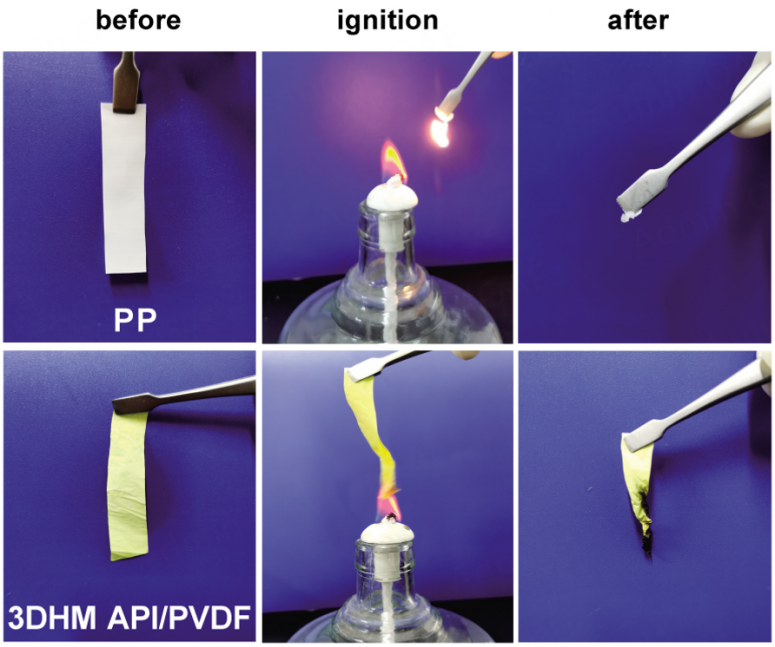

Figure 6. Digital photos showing flammability of PP and 3DHM API/PVDF separators.

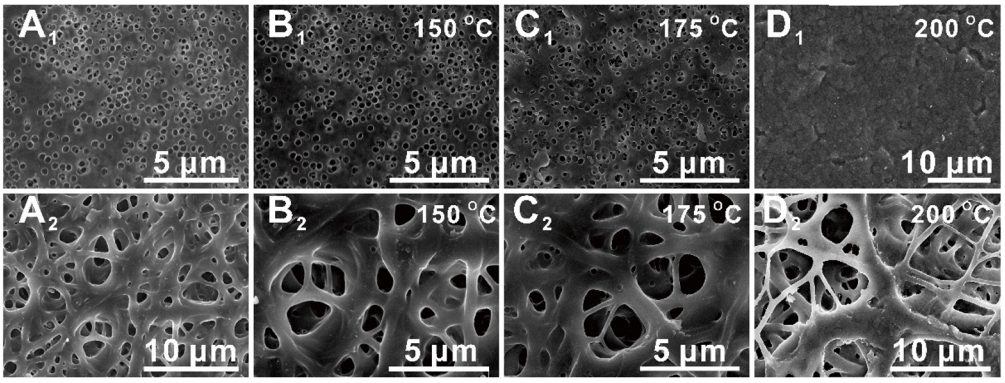

Figure 7. The modified side and unmodified side SEM images of 3DHM API/PVDF separators before and after the thermal treatments for 30 min.

discrepancy between the temperature at which the shutdown and meltdown temperature of the separator occurs is approximately 100 °C. This ensures that the LIB is safe for use.

As shown in Figure 8A, the tensile strength of the PI membrane was 22.2 MPa in the vertical direction and 21.3 MPa in the transverse direction, respectively. The PVDF coating on the PI membrane elevated the tensile strength to 41.0 MPa, which would facilitate the operability of the 3DHM API/PVDF in lithium battery assembly. The porosity of PP is 62.7%, while that of 3DHM API/PVDF is 80.8% [Figure 8B], indicating an improved capacity for liquid electrolyte uptake. The PVDF coating on one side of the separator can help retain the electrolyte and promote the transport of Li^+ ions. The pore size distribution of PP and 3DHM API/PVDF is presented in Supplementary Figure 2. The average PP separator pore size is 0.088 μm, which is in close proximity to the data provided by the manufacturer (0.064 μm). The pore size distribution of 3DHM API/PVDF exhibits two peaks. The first peak, at 100 nm, corresponds to the

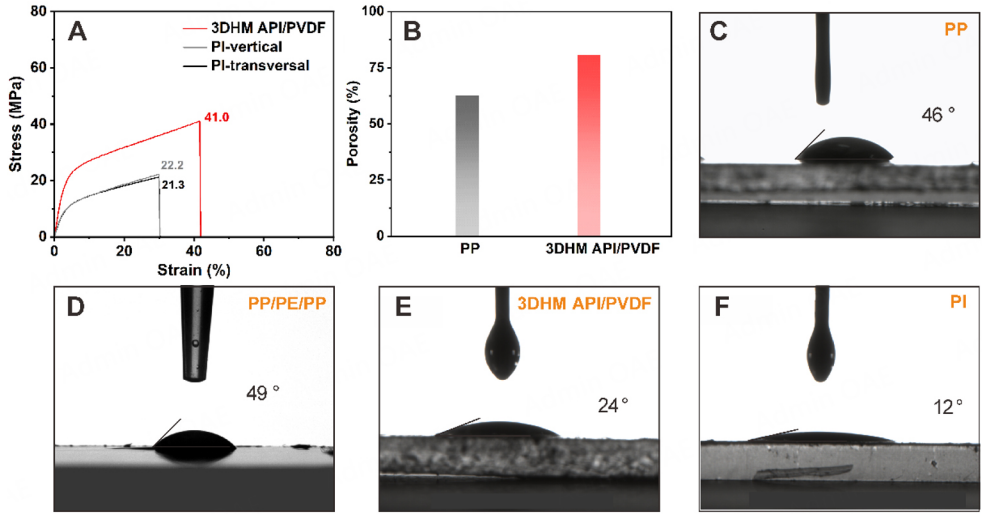

Figure 8. Stress-strain curves (A) and porosity (B) of PP and 3DHM API/PVDF. Contact angle for PP, PP/PE/PP separator, 3DHM API/PVDF membrane and PI film. (C) PP separator, (D) PP/PE/PP separator, (E) 3DHM API/PVDF membrane and (F) PI film.

modification layer. The value is smaller than the particle size of the silica template (300 nm), which may be attributed to the presence of multilayer stacking. However, if the PVDF coating is very thin, it may be possible to detect pores of 300 nm. The 1 μm pore in 3DHM API/PVDF is derived from the PI membrane. Sufficient electrolyte wetting in LIBs has been pointed out as a critical factor, which helps to maintain its endurance and facilitates smooth diffusion[34]. The contact angle was used to characterize the wettability of the separator in the electrolyte. The height between the needle points of the dropper and the separator was ~2 mm. The angle was measured and recorded as soon as the electrolyte contacts the separator interface. Figure 8C-E shows that the contact angles of PP and PP/PE/PP are 46° and 49°, respectively, while that of 3DHM API/PVDF is 24°. It can be concluded that the electrolyte is more easily absorbed by the 3DHM API/PVDF membrane than by the PP separator. The outstanding affinity of the PVDF polymer for electrolyte solutions makes this possible, which is inherent to the material[35]. The contact angle significantly decreases to 12° for the PI film [Figure 8F], indicating the increase in the wettability of the base film with the electrolyte. Therefore, the 3DHM API/PVDF membrane exhibits good wettability, which accelerates the infiltration of electrolyte.

As shown in Figure 9A, the electrolyte uptake of 3DHM API/PVDF is 494%, whereas that of PP is only 320%. Figure 9B illustrates the impedance spectra of batteries utilizing PP and 3DHM API/PVDF, respectively. The ionic conductivity of PP and 3DHM API/PVDF is 0.65 and 0.68 mS cm^{-1}, respectively [Figure 9C]. It is evident that 3DHM API/PVDF exhibits enhanced ionic conductivity compared to PP, attributed to its superior wetting performance and enhanced Li^+ ion transport. The change in impedances and ionic conductivity at different elevated temperatures clearly reflect the temperature-responsive behavior of the separators. Figure 9D and E illustrates the impedance of the PP and 3DHM API/PVDF across a temperature range of 60 to 200 °C. As displayed in Figure 9D, the blank PP separator exhibits a Z' value of 55.1 Ω at 60 °C, which is slightly diminished to 34.7 Ω at 90 °C. The viscosity reduction of the liquid electrolyte at elevated temperatures can be attributed to this phenomenon. Further increases in temperature to 120 °C result in an internal short circuit in the cell, potentially attributable to thermal shrinkage of the PP. This finding is consistent with the results of thermal stability testing. As displayed in Figure 9E, the 3DHM API/PVDF separator exhibits a Z' value of 6.45 Ω at 60 °C, followed by a gradual decline to 4.0, 1.73, and 1.72 Ω at 90, 120, and 150 °C, respectively. The lower impedance value indicates that the 3DHM API/PVDF

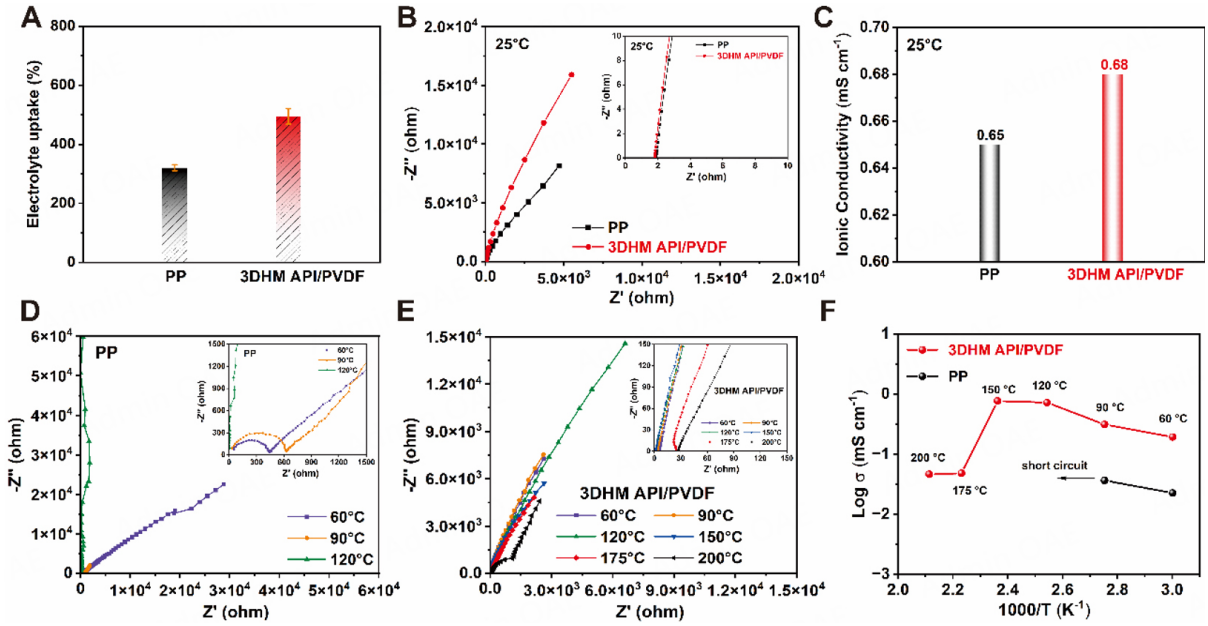

Figure 9. (A) Electrolyte uptake of PP and 3DHM API/PVDF. Impedance spectra (B) and ionic conductivity (C) of PP and 3DHM API/PVDF at 25 °C. (D) Impedance spectra of PP separator at 60 to 120 °C (Inset is an enlarged view). (E) Impedance spectra of 3DHM API/PVDF separator at 60 to 200 °C (Inset is an enlarged view). (F) Temperature-dependence ionic conductivity of PP and 3DHM API/PVDF.

has superior compatibility with the liquid electrolyte than PP. However, the Z' value increases to 25.8 Ω at 175 °C, possibly due to the melting of PVDF and the shutdown function of the separator. This value further increases to 26.8 Ω at 200 °C due to the further shutdown of the pores. Figure 9F summarizes the ionic conductivity of PP and 3DHM API/PVDF at high temperatures. The cell assembled with 3DHM API/PVDF did not exhibit any internal short circuits during the test temperature, which can be attributed to the excellent thermal stability of 3DHM API/PVDF.

The dendrite-suppressing capability of separators was tested in Li symmetric cells at a current density of 0.2 mA cm^{-2} and a capacity of 0.2 mAh cm^{-2}, as illustrated in Figure 10. Figure 10A provides clear evidence that the polarization voltage of the PP-based cell is greater than that of the 3DHM API/PVDF-based cell. This suggests that the 3DHM API/PVDF membrane is more conducive to lithium-ion transport. The lithium stripping/plating behaviors of the PP and 3DHM API/PVDF were further investigated at 1.0 mA cm^{-2} [Figure 10B]. The cell with a 3DHM API/PVDF separator demonstrates good cycling stability with a cycle life of 2,000 h. In contrast, the cell with a PP separator exhibits a significantly larger voltage polarization and short circuit only after cycling for 410 h. This phenomenon can be attributed to the repeated growth and corrosion of lithium dendrites, which result in an electrical disconnection and depletion of electrolyte[36]. The difference in cycle stability demonstrates the superiority of the 3DHM structure of the as-fabricated separator for repeated plating and stripping of Li. In order to illustrate the advantages of the 3DHM API/PVDF separator for lithium plating, the morphologies of lithium-metal electrodes were imaged by SEM after charging/discharging. Figure 10C and D shows that the lithium deposition morphology with the 3DHM API/PVDF film is lumpy-shaped and denser, without any sharp lithium dendrites. In contrast, loose and uneven spaghetti lithium dendrites grew on the lithium metal electrode while the PP separator was in the battery. This irregular growth of lithium dendrites is primarily due to a lack of lithium precipitation control[37]. Figure 11 illustrates the diverse transmission pathways of lithium ions and the thermal response characteristics of the PP and 3DHM API/PVDF.

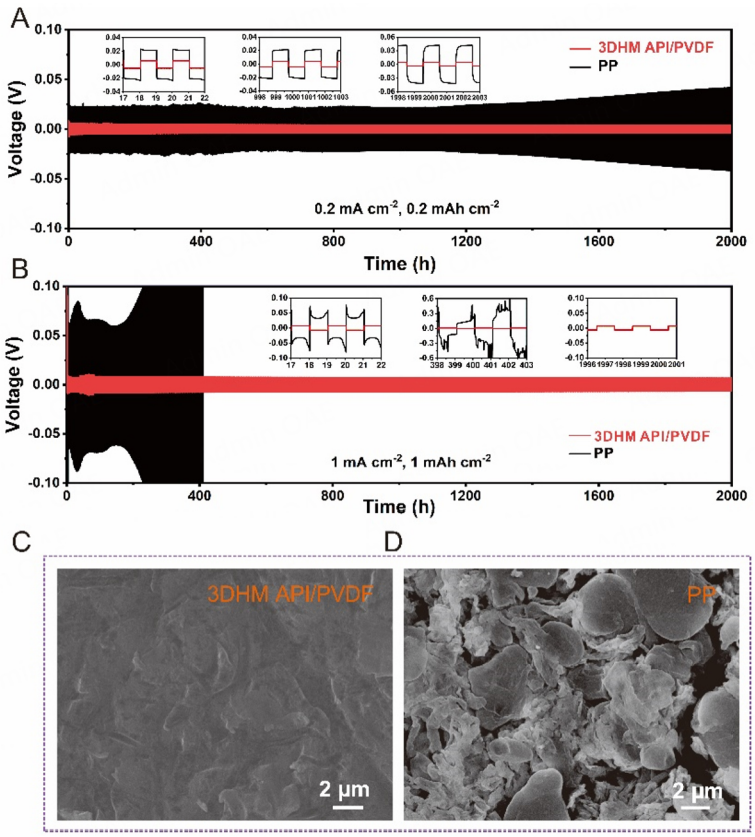

Figure 10. Cycle performance of Li symmetric cells using 3DHM API/PVDF and PP with a current density of 0.2 mA cm^{-2} (A) and 1.0 mA cm^{-2} (B). SEM images of the surface of the cycled lithium foil in the symmetrical lithium metal cells at 0.2 mA cm^{-2} for 60 cycles with (C) 3DHM API/PVDF and (D) PP films.

A comparative investigation was conducted on the cycling and rate performance of the NCA/Li coin cell with 3DHM API/PVDF or PP separators. The objective of this investigation was to evaluate the effects of the modified separator on the electrochemical performance of the cells. As can be seen in Figure 12, the first discharge capacity of the 3DHM API/PVDF separator-based battery is ~172 mA hg^{-1} at the current density of 0.1 C, which is comparable with a PP membrane [Figure 12A and B]. The 3DHM API/PVDF separators show higher cycling stability than PP separators displayed in Figure 12C with a discharge capacity of ~120 mA hg^{-1} after 200 charge/discharge cycles. The reason for cycling stability improvement may be that the interconnected microporous structure promotes Li^+ transport and uniform disposition of Li^+. The NCA/Li cells with 3DHM API/PVDF separators demonstrated a capacity of 170, 165, 155, 140, 115, and 80 mAh g^{-1}, corresponding to 0.2, 0.5, 1, 2, 5, and 10 C, respectively [Figure 12D]. The decay in the 10 C capability of the cells can be attributed to the high thickness of a modified layer, which enlarges the ionic conduction distance between electrodes. The performance of NCA/3DHM API/PVDF/Li was also compared with other reported thermal shutdown functionalized separators [Supplementary Table 1]. The performance of NCA/3DHM API/PVDF/Li was superior to that of some of the reported results. These results indicate that the modified 3DHM API/PVDF separator does not significantly impede the transport of Li^+ at room temperature. The open circuit voltage of the NCA/3DHM API/PVDF/Li was tested following a one-hour treatment at temperatures ranging from 25 to 150 °C [Supplementary Figure 3]. No abrupt voltage change was observed, indicating that a short circuit did not occur. The results demonstrate that the 3DHM API/PVDF exhibits no shrinkage at a high temperature of 150 °C, which enhances the safety of the cell.

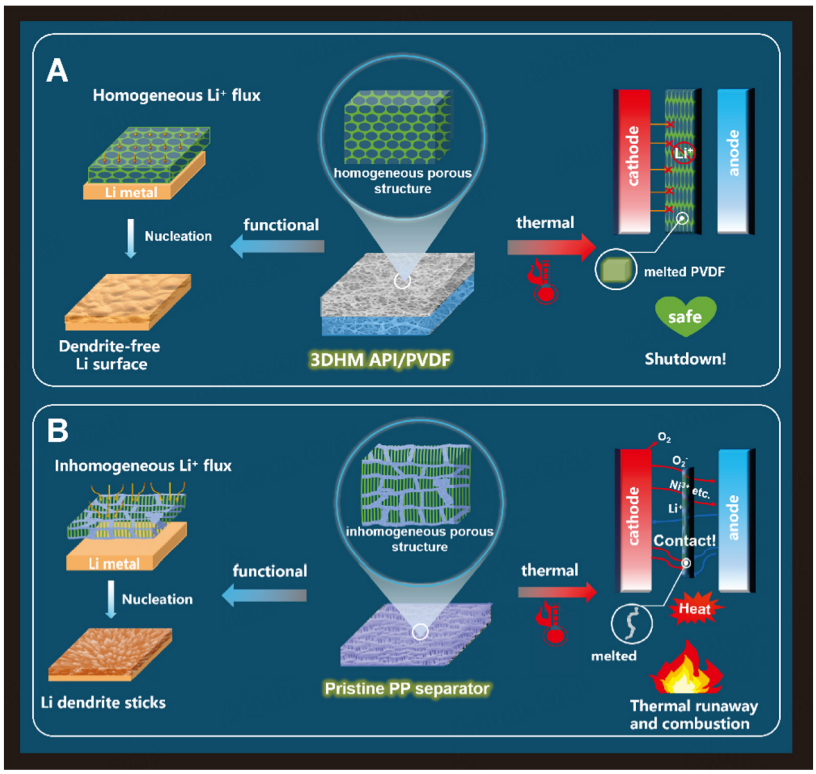

Figure 11. The different transmission routes of lithium ions and the thermal response characteristics of the PP and 3DHM API/PVDF.

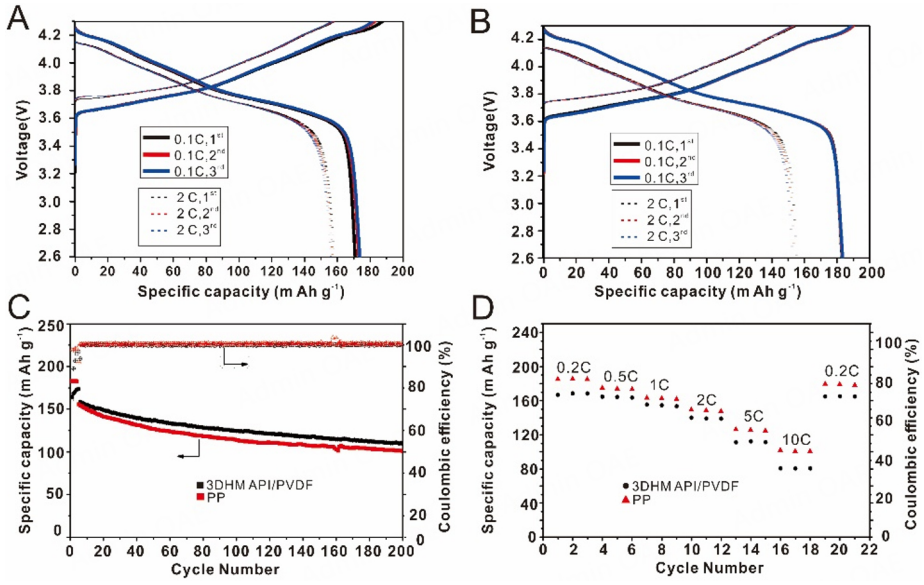

Figure 12. The electrochemical performance of the NCA/separator/Li battery with a 3DHM API/PVDF separator and a PP membrane at 25 °C. The charge-discharge curves of batteries with (A) 3DHM API/PVDF separator and (B) PP membrane at rates of 0.1 and 2 C. (C) the cycle performance and (D) the rate performance of the battery.

PVDF-HFP is another extensively studied polymer for LIBs due to its special porous and semicrystalline structure[38]. To preliminarily test the general applicability of the design, PVDF was replaced by PVDF-HFP, and 3DHM API/PVDF-HFP was obtained. As shown in Supplementary Figures 4 and 5, the morphologies

and structures of API/PVDF-HFP-SiO_2 and 3DHM API/PVDF-HFP are similar to API/PVDF-SiO_2 and 3DHM API/PVDF. The melting temperature of 3DHM API/PVDF-HFP was 135 °C, and after the thermal treatment at 150 °C for 0.5 h, the modified layer had already melted [Supplementary Figures 6-10]. The NCA/3DHM API/PVDF-HFP separator /Li battery has also been assembled. The first discharge capacity of the cell is approximately 182 mA hg^{-1} at a current density of 0.1 C [Supplementary Figure 11]. The 3DHM API/PVDF-HFP separator also shows high cycling stability.

CONCLUSIONS

In summary, we prepared 3DHM API/PVDF separators. The 3DHM structure can ensure high-speed ion conductivity and homogeneous Li dispersion and suppress the dendrite growth. The incorporation of a PVDF layer imbues the separator with a thermal shutdown function at 175 °C, resulting from the material's melting and formation of a pore-free film. This thermal stability is evidenced by the membrane's lack of discernible shrinkage even at 275 °C, with the temperature differential between the shutdown and meltdown temperatures exceeding 100 °C to safeguard the safe utilization of LIBs. This work presents a strategy that combines a 3DHM structure, a functional polymeric coating, and a thermal stable membrane to prepare the separator compatible with high-security LIBs with a thermal shutdown function. The novel 3DHM API/PVDF separator may be a promising candidate for a safer LIB.

DECLARATIONS

Authors' contributions

Research design and funding acquisition: Jin Y
Writing-original draft: Chang H
Data collection and experiment: Zhang Z, Chang H, Kang G
Data collection and analysis: Zhang Z, Chang H, Kang G
Review and editing: Jin Y, Zhang Z, Liu W
Refining the ideas and finalizing this paper: Jin Y, Zhang Z, Chang H

Availability of data and materials

The data are made available upon request to authors.

Financial support and sponsorship

This work was financially supported by the National Natural Science Foundation of China (52172245), the Key Scientific and Technological Innovation Project of Shandong (No. 2020CXGC010401), and the Major Basic Research Projects of the Shandong Natural Science Foundation (No. ZR2020ZD07).

Conflicts of interest

All authors declared that there are no conflicts of interest.

Ethical approval and consent to participate

Not applicable.

Consent for publication

Not applicable.

REFERENCES

1. Scrosati B, Garche J. Lithium batteries: status, prospects and future. *J Power Sources* 2010;195:2419-30. DOI
2. Tian X, Yi Y, Fang B, et al. Design strategies of safe electrolytes for preventing thermal runaway in lithium ion batteries. *Chem Mater* 2020;32:9821-48. DOI
3. Cho T, Tanaka M, Ohnishi H, et al. Composite nonwoven separator for lithium-ion battery: development and characterization. *J Power Sources* 2010;195:4272-7. DOI
4. Kim M, Park JH. Inorganic thin layer coated porous separator with high thermal stability for safety reinforced Li-ion battery. *J Power Sources* 2012;212:22-7. DOI
5. Cheng XB, Zhang R, Zhao CZ, Wei F, Zhang JG, Zhang Q. A review of solid electrolyte interphases on lithium metal anode. *Adv Sci* 2016;3:1500213. DOI
6. Zheng G, Lee SW, Liang Z, et al. Interconnected hollow carbon nanospheres for stable lithium metal anodes. *Nat Nanotechnol* 2014;9:618-23. DOI
7. Ma F, Zhang Z, Yan W, et al. Solid polymer electrolyte based on polymerized ionic liquid for high performance all-solid-state lithium-ion batteries. *ACS Sustain Chem Eng* 2019;7:4675-83. DOI
8. Chen D, Liu T, Zhou X, Tjiu WC, Hou H. Electrospinning fabrication of high strength and toughness polyimide nanofiber membranes containing multiwalled carbon nanotubes. *J Phys Chem B* 2009;113:9741-8. DOI PubMed
9. Dong G, Sun G, Tian G, Qi S, Wu D. Robust polyimide nanofibrous membrane with bonding microstructures fabricated via dipping process for lithium-ion battery separators. *Energy Technol* 2019;7:1801072. DOI
10. Dong G, Liu B, Sun G, Tian G, Qi S, Wu D. TiO_2 nanoshell@polyimide nanofiber membrane prepared via a surface-alkaline-etching and in-situ complexation-hydrolysis strategy for advanced and safe LIB separator. *J Membr Sci* 2019;577:249-57. DOI
11. Dong G, Dong N, Liu B, Tian G, Qi S, Wu D. Ultrathin inorganic-nanoshell encapsulation: TiO_2 coated polyimide nanofiber membrane enabled by layer-by-layer deposition for advanced and safe high-power LIB separator. *J Membr Sci* 2020;601:117884. DOI
12. Elia GA, Ducros JB, Sotta D, et al. Polyacrylonitrile separator for high-performance aluminum batteries with improved interface stability. *ACS Appl Mater Interfaces* 2017;9:38381-9. DOI PubMed
13. Liu J, Liu Y, Yang W, Ren Q, Li F, Huang Z. Lithium ion battery separator with high performance and high safety enabled by tri-layered SiO_2@PI/m-PE/SiO_2@PI nanofiber composite membrane. *J Power Sources* 2018;396:265-75. DOI
14. Shi C, Dai J, Shen X, et al. A high-temperature stable ceramic-coated separator prepared with polyimide binder/Al_2O_3 particles for lithium-ion batteries. *J Membr Sci* 2016;517:91-9. DOI
15. Zhu C, Nagaishi T, Shi J, et al. Enhanced wettability and thermal stability of a novel polyethylene terephthalate-based poly(vinylidene fluoride) nanofiber hybrid membrane for the separator of lithium-ion batteries. *ACS Appl Mater Interfaces* 2017;9:26400-6. DOI
16. Battery properties of Li-ion battery with non-woven fabric separators. The 51th Battery Symposium in Japan, Nagoya 2010, 1b25.
17. Nishikawa S. Characterization of aramid coated fine porous pe separator. The 47th Battery Symposium in Japan, Tokyo 2006, 2e06.
18. Jung YS, Cavanagh AS, Gedvilas L, et al. Improved functionality of lithium-ion batteries enabled by atomic layer deposition on the porous microstructure of polymer separators and coating electrodes. *Adv Energy Mater* 2012;2:1022-7. DOI
19. Jiang W, Liu Z, Kong Q, et al. A high temperature operating nanofibrous polyimide separator in Li-ion battery. *Solid State Ion* 2013;232:44-8. DOI
20. Sun G, Liu B, Niu H, et al. In situ welding: superb strength, good wettability and fire resistance tri-layer separator with shutdown function for high-safety lithium ion battery. *J Membr Sci* 2020;595:117509. DOI
21. Tan J, Kong L, Qiu Z, Yan Y. Flexible, high-wettability and thermostable separator based on fluorinated polyimide for lithium-ion battery. *J Solid State Electrochem* 2018;22:3363-73. DOI
22. Wu D, Shi C, Huang S, et al. Electrospun nanofibers for sandwiched polyimide/poly (vinylidene fluoride)/polyimide separators with the thermal shutdown function. *Electrochim Acta* 2015;176:727-34. DOI
23. Zhang H, Lin C, Zhou M, John AE, Zhu B. High thermal resistance polyimide separators prepared via soluble precusor and non-solvent induced phase separation process for lithium ion batteries. *Electrochim Acta* 2016;187:125-33. DOI
24. Lu Z, Sui F, Miao Y, et al. Polyimide separators for rechargeable batteries. *J Energy Chem* 2021;58:170-97. DOI
25. Zhang C, Li H, Wang S, et al. A polyethylene microsphere-coated separator with rapid thermal shutdown function for lithium-ion batteries. *J Energy Chem* 2020;44:33-40. DOI
26. Wang B, Prinsen P, Wang H, et al. Macroporous materials: microfluidic fabrication, functionalization and applications. *Chem Soc Rev* 2017;46:855-914. DOI
27. Ma D, Cao Z, Wang H, Huang X, Wang L, Zhang X. Three-dimensionally ordered macroporous FeF_3 and its in situ homogenous polymerization coating for high energy and power density lithium ion batteries. *Energy Environ Sci* 2012;5:8538-42. DOI
28. Hatton B, Mishchenko L, Davis S, Sandhage KH, Aizenberg J. Assembly of large-area, highly ordered, crack-free inverse opal films. *Proc Natl Acad Sci USA* 2010;107:10354-9. DOI PubMed PMC
29. Phillips KR, England GT, Sunny S, et al. A colloidoscope of colloid-based porous materials and their uses. *Chem Soc Rev* 2016;45:281-322. DOI
30. Stein A, Wilson BE, Rudisill SG. Design and functionality of colloidal-crystal-templated materials-chemical applications of inverse opals. *Chem Soc Rev* 2013;42:2763-803. DOI PubMed
31. Lee H, Yanilmaz M, Toprakci O, Fu K, Zhang X. A review of recent developments in membrane separators for rechargeable lithium-

ion batteries. *Energy Environ Sci* 2014;7:3857-86. DOI

32. Laman FC, Gee MA, Denovan J. Impedance studies for separators in rechargeable lithium batteries. *J Electrochem Soc* 1993;140:L51-3. DOI
33. Abraham K. Directions in secondary lithium battery research and development. *Electrochim Acta* 1993;38:1233-48. DOI
34. Zhang SS. A review on the separators of liquid electrolyte Li-ion batteries. *J Power Sources* 2007;164:351-64. DOI
35. Wu D, Huang S, Xu Z, et al. Polyethylene terephthalate/poly (vinylidene fluoride) composite separator for Li-ion battery. *J Phys D Appl Phys* 2015;48:285305. DOI
36. Cheng XB, Peng HJ, Huang JQ, Zhang R, Zhao CZ, Zhang Q. Dual-phase lithium metal anode containing a polysulfide-induced solid electrolyte interphase and nanostructured graphene framework for lithium-sulfur batteries. *ACS Nano* 2015;9:6373-82. DOI PubMed
37. Ju Z, Nai J, Wang Y, et al. Biomacromolecules enabled dendrite-free lithium metal battery and its origin revealed by cryo-electron microscopy. *Nat Commun* 2020;11:488. DOI PubMed PMC
38. Li H, Ding Y, Ha H, et al. An all-stretchable-component sodium-ion full battery. *Adv Mater* 2017;29:1700898. DOI